J Eng Math (2009) 65:243–255
DOI 10.1007/s10665-009-9310-2

Coated photonic crystals: computation of the Green tensor and analysis of the bandgap

F. Seydou · Omar M. Ramahi · T. Seppänen

Received: 18 February 2009 / Accepted: 8 June 2009 / Published online: 14 July 2009

Abstract A finite-size two-dimensional photonic crystal composed of dielectric rods with holes centered within each rod is considered. The geometry of the rods, as well as the holes, is of arbitrary shape. A boundary-element method is implemented for computing the Green tensor. The semi-analytical solution is used for validating the numerical results in the case of circular geometry. Different types of configurations and geometry shapes are considered in the computation.

Keywords Boundary integral · Layer potential · Photonic crystal

1 Introduction

A photonic crystal (PC) is a periodic structure that has bandgap (a range of prohibited frequencies for the propagation of electromagnetic waves inside).

Initially, much theoretical and experimental research in photonic crystals was carried out to calculate band diagrams (the solution of the eigen problem associated with Maxwell's equation) and find the transmission and reflection spectra of such structures. This, however, provides little insight into the ways in which a PC modifies the electromagnetic vacuum. This modification is seen from the computation of the Green tensor [1].

The existence of bandgap can be seen by the changes in the local density of states (LDOS), which is a function of the Green tensor. In particular, for infinite structures, the LDOS vanishes inside a complete bandgap. For finite-size crystals encountered in realistic situations, the LDOS for gap wavelengths is small but does not vanish.

Arrays of air-holes in a dielectric background and that of dielectric rods in an air background are the most commonly found PCs in the literature. Recently a new type of structure called annular PC, composed of coated materials, such as a dielectric background with an air-hole array and dielectric rods centered within each air-hole, has drawn attention. If they could be designed, such crystals would have important technological applications [1–4].

Many simulation methods have been applied to study photonic crystals, including boundary-integral-based methods [5,6], the transition matrix approach [1] and finite-element methods [7]. The T-matrix method has been

F. Seydou (✉) · T. Seppänen
Department of Electrical and Information Engineering, University of Oulu, Oulu, Finland
e-mail: fadseydou@nepadcouncil.org

O. M. Ramahi
Department of Electrical and Computer Engineering, University of Waterloo, Waterloo, ON, Canada

developed to compute the transmission characteristics and the bandgap structure for circularly coated photonic structures [8]. Numerical computation, based on layer potentials, for analyzing the bandgap in the case of annular crystals of arbitrary shape has not been considered so far, to the best of our knowledge. In this paper we discuss a boundary-integral method for computing the Green tensor for a two-dimensional (2D) coated PC of arbitrary shape. In particular, we consider a finite-size PC composed of an array of dielectric rods in an air background such that holes are centered within each dielectric rod. Thus, the clusters we consider consist of parallel, disjoint two-layered cylinders of arbitrary shape. We implement the computational techniques and analyze the Green tensor, using both the semi-analytical (for circular cylinders) and numerical boundary-element (for arbitrarily shaped cylinders) methods, for a source at location $\mathbf{x}_s$ and observation point at $\mathbf{x}$. The source, a line antenna of infinite length parallel to the cylinder axes, radiates with harmonic time dependence. The polarizations of the electromagnetic waves decouple to TM and TE polarizations. The semi-analytical method [1] will be used to validate the numerical algorithm.

The boundary-element technique developed in this paper uses potential theory and Green identities (cf. [9,10]), and can be easily applied to other annular PC types considered in the literature. The boundary integrals use the free-source Green's function and inherits from its properties. The method requires matrix–vector multiplications, which can be efficiently done by available fast multipole methods.

Our results show an excellent match between the semi-analytical [1] and the numerical methods. Our numerical method is computationally efficient and can be implemented with short computation time.

2 Formulation of the problem

We consider a harmonic electromagnetic problem with wavelength λ and frequency ω, where the wave number is given by $k = \omega/c = 2\pi/\lambda$. The constant c represents the speed of light.

We wish to compute the electric-field Green tensor (the electric-field response to a source) in a photonic crystal (PC), for a source at $\mathbf{x}_s = (x_s, y_s, z_s)$ and observation point at $\mathbf{x} = (x, y, z)$. The Green tensor is a second-rank tensor with 3×3 components [11]. The elements in column u represent the components of the electric field vector (G_{xu}, G_{yu}, G_{zu}) generated by a source radiating, with harmonic time dependence $\exp(-\mathrm{i}\omega t)$, parallel to the $u = x, y, z$ axes, respectively.

The PC under consideration consists of a finite number (M) of infinite dielectric rods of arbitrary shape $\tilde{D}_l$, $l = 1, 2, \ldots, M$, transverse to the $\mathbf{x} = (x, y)$-plane. Each rod $\tilde{D}_l$ contains a hole $\Omega_l^2, l = 1, 2, \ldots, M$. The annulus between the two regions is denoted by $\Omega_l^1 = \tilde{D}_l \backslash \overline{\Omega_l^2}$. The region outside the rods is denoted by $\Omega_0 = \mathbf{R}^2 \backslash \cup_{l=1}^{M} (\overline{\tilde{D}_l})$, and the medium is characterized by the refractive index $\nu(\mathbf{x})$. In Fig. 1 we represent a finite-size annular PC consisting

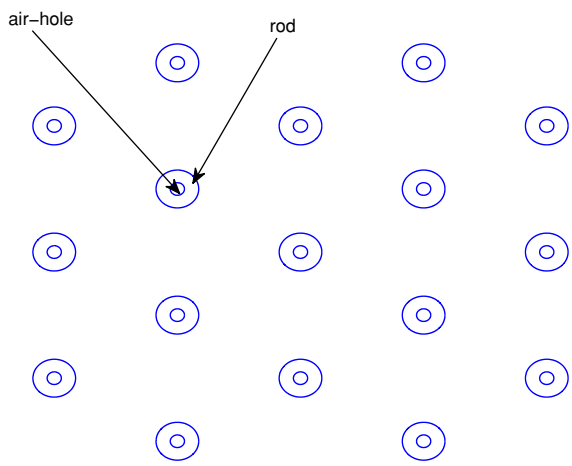

Fig. 1 A finite-size annular PC consisting of 17 rods with holes

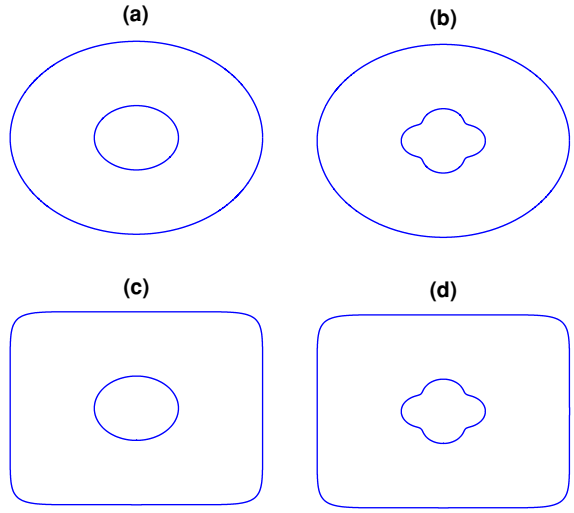

Fig. 2 The computations are made for four configurations: **a** the rods and the holes are circular 'CC'; **b** The rods are circular and the holes are deformed circles 'CD'; **c** the rods are square and the holes are circular 'SC'; **d** the rods are square and the holes are deformed circles 'SD'

of 17 circular dielectric cylinders with circular holes. In Fig. 2 we describe the different configurations (CC, CD, SC and SD) of the geometry that we will use in our numerical computation. We have used squares with rounded corners for ensuring an exponential convergence in our result, but the results are not affected by this approximation.

Since we consider a two-dimensional in-plane problem, the vector character of the fields in the Maxwell equations implies that one has to distinguish two possible polarization directions with differing boundary conditions. The situation where the electric (resp. magnetic) field is parallel to the cylinders (z)-axis is called TM (resp. TE) polarization, with the magnetic (resp. electric) field thus being transverse.

For TM polarization the Green tensor reduces to a form involving only a single non-trivial scalar $G^{\mathrm{TM}} = G_{zz}$, while for TE polarization it reduces to a 2×2 tensor form $G^{\mathrm{TE}} = (G_{xu}, G_{yu})$, u representing x or y, [11].

Before we try and find the components of the Green tensor for the PC structure presented above we will first give the mathematical formulation of the problem, considering the case in which the source is located outside as well as that when it is inside the cylinders.

2.1 The case of TM polarization

For TM polarization the Green tensor $G^{\mathrm{TM}} = G_{zz}(\mathbf{x}, \mathbf{x}_s)$ satisfies the following equation [12],

$$\nabla^2 G^{\mathrm{TM}} + k^2 \nu G^{\mathrm{TM}} = \delta(\mathbf{x} - \mathbf{x}_s), \tag{1}$$

where δ is the Dirac delta function. We assume further that the refractive index ν and the Green tensor are given, for $l = 1, 2 \ldots, M$, and $j = 1, 2$, by

$$\Big(\nu(\mathbf{x}), G^{\mathrm{TM}}(\mathbf{x})\Big) = \begin{cases} (\nu_l^j, G_l^{\mathrm{TM},j}(\mathbf{x})), & \mathbf{x} \in \Omega_l^j, \\ (\nu_0, G_0^{\mathrm{TM}}(\mathbf{x})), & \mathbf{x} \in \Omega_0, \end{cases}$$

where ν_l^j and ν_0 are real positive constants, with $\nu_l^j > 1$.

We have continuity conditions (cf. [5]), for G^{TM} and its normal derivative, on the boundary of $\tilde{D}_l$, the interface Γ_l^1 between Ω_0 and each rod $\tilde{D}_l$, and on the interface Γ_l^2 (the boundary of Ω_l^2) between the hole Ω_l^2 and Ω_l^1, $l = 1, 2, \ldots, M$, i.e., we have the following boundary conditions:

$$G_l^{\mathrm{TM},2} = G_l^{\mathrm{TM},1} \quad \text{and} \quad \frac{\partial}{\partial \mathbf{N}} G_l^{\mathrm{TM},2} = \frac{\partial}{\partial \mathbf{N}} G_l^{\mathrm{TM},1}, \quad \text{on } \Gamma_l^2, \tag{2}$$

and

$$G_0^{\mathrm{TM}} = G_l^{\mathrm{TM},1} \quad \text{and} \quad \frac{\partial}{\partial \mathbf{N}} G_0^{\mathrm{TM}} = \frac{\partial}{\partial \mathbf{N}} G_l^{\mathrm{TM},1}, \quad \text{on } \Gamma_l^1, \tag{3}$$

where $\mathbf{N}$ is the unit normal which is assumed to be directed towards the exterior.

Let us introduce the fundamental solution to the Helmholtz equations in free space as

$$\Phi_l^j(\mathbf{x}, \mathbf{x}') = -\frac{\mathrm{i}}{4} H_0^{(1)}(\kappa_l^j |\mathbf{x} - \mathbf{x}'|), \quad l = 1, 2, \ldots, M, \quad \text{and} \quad j = 1, 2,$$

where $\kappa_l^j = k\sqrt{\nu_l^j}$, and $H_0^{(1)}$ is the Hankel function of the first kind and order zero. We also use the notation $\Phi_0(\mathbf{x}, \mathbf{x}') = -\mathrm{i} H_0^{(1)}(k\sqrt{\nu_0}|\mathbf{x} - \mathbf{x}'|)/4$.

Now, for $l = 1, \ldots, M$, and $j = 1, 2$, define in Ω_l^j,

$$u_l^j(\mathbf{x}) = G_l^{\mathrm{TM},j}(\mathbf{x}) - \xi_l^{\mathrm{int},j} \Phi_l^j(\mathbf{x}, \mathbf{x}_s),$$

where $\xi_l^{\mathrm{int},j} = 1$ (resp. $\xi_l^{\mathrm{int},j} = 0$) if $\mathbf{x}_s$ lies in Ω_l^j (resp. outside of Ω_l^j). Define in the exterior

$$u_0(\mathbf{x}) = G_0^{\mathrm{TM}}(\mathbf{x}) - \xi^{\mathrm{ext}} \Phi_0(\mathbf{x}, \mathbf{x}_s),$$

where $\xi^{\mathrm{ext}} = 1$ (resp. $\xi^{\mathrm{ext}} = 0$) if $\mathbf{x}_s$ lies in Ω_0 (resp. otherwise). Since Φ satisfies Eq. 1 with $\mathbf{x}'$ replaced by $\mathbf{x}_s$ we have,

$$\nabla^2 u_l^j + k^2 \nu_l^j u_l^j = 0 \quad \text{in } \Omega_l^j, \quad l = 1, 2, \ldots, M, \quad \text{and} \quad j = 1, 2, \tag{4}$$

$$\nabla^2 u_0 + k^2 \nu_0 u_0 = 0 \quad \text{in } \Omega_0. \tag{5}$$

The boundary conditions (2) and (3) give, for $l = 1, 2, \ldots, M$,

$$u_l^1 - u_l^2 = f_l^{1,2} \quad \text{and} \quad \frac{\partial}{\partial \mathbf{N}}(u_l^1 - u_l^2) = \frac{\partial f_l^{1,2}}{\partial \mathbf{N}}, \quad \text{on } \Gamma_l^2, \tag{6}$$

and

$$u_l^1 - u_0 = f_l^{1,0} \quad \text{and} \quad \frac{\partial}{\partial \mathbf{N}}(u_l^1 - u_0) = \frac{\partial f_l^{1,0}}{\partial \mathbf{N}} \quad \text{on } \Gamma_l^1, \tag{7}$$

where

$$f_l^{1,2} = \xi_l^{\mathrm{int},2} \Phi_l^2 - \xi_l^{\mathrm{int},1} \Phi_l^1$$

$$f_l^{1,0} = \xi^{\mathrm{ext}} \Phi_0 - \xi_l^{\mathrm{int},1} \Phi_l^1$$

In addition, we assume the Sommerfeld radiation condition for u_0, i.e.,

$$\lim_{|\mathbf{x}| \to \infty} |\mathbf{x}|^{1/2} \left(\frac{\partial u_0}{\partial |\mathbf{x}|} - \mathrm{i} k \nu_0 u_0 \right) = 0. \tag{8}$$

So, to obtain the Green tensor in (1), we solve the problem (4)–(8) to obtain u_l, then $G_l^{\mathrm{TM},j} = u_l^j + \xi_l^{\mathrm{int},j} \Phi_l^j$, for $l = 1, 2, \ldots, M$ and $j = 1, 2$; and u_0, then $G_0^{\mathrm{TM}} = u_0 + \xi^{\mathrm{ext}} \Phi_0$.

2.2 The case of TE polarization

For TE polarization, the process is similar (but less direct) to the TM case and requires the solution of two scalar problems for $G^{\mathrm{TE},u} = (G_{xu}, G_{yu})$, where $u = x, y$ [12]. The components of the Green tensor are electric field quantities derived from the magnetic field $G^{M,u}$, generated by a current source, according to

$$G_{xx} = \frac{\mathrm{i}}{k\nu_0} \frac{\partial G^{M,x}}{\partial y}, \quad G_{yx} = \frac{-\mathrm{i}}{k\nu_0} \frac{\partial G^{M,x}}{\partial x}, \tag{9}$$

$$G_{xy} = \frac{\mathrm{i}}{k\nu_0} \frac{\partial G^{M,y}}{\partial y}, \quad G_{yy} = \frac{-\mathrm{i}}{k\nu_0} \frac{\partial G^{M,y}}{\partial x}, \tag{10}$$

where

$$\nabla^2 G^{M,x} + k^2 \nu G^{M,x} = \frac{\mathrm{i}}{k}\frac{\partial}{\partial y}\delta(\mathbf{x}-\mathbf{x}_s) \quad \text{and} \quad \nabla^2 G^{M,y} + k^2 \nu G^{M,y} = -\frac{\mathrm{i}}{k}\frac{\partial}{\partial x}\delta(\mathbf{x}-\mathbf{x}_s). \tag{11}$$

Similarly to the TM case, it is straightforward to derive from (11), for $G^{M,x}$ (resp. $G^{M,y}$) the same type of equations like in (4)–(8), by replacing Φ with $\Phi^x = -H_1^{(1)}(\kappa\sqrt{\nu}|\mathbf{x}-\mathbf{x}'|)\sin(\theta)/4$ (resp. $\Phi^y = H_1^{(1)}(\kappa\sqrt{\nu}|\mathbf{x}-\mathbf{x}'|)\cos(\theta)/4$), and taking into account that for the TE case we have continuity of G^M and $\mathbf{N}\cdot\nabla G^M/\nu$. Here $\theta = \arg(\mathbf{x}-\mathbf{x}')$. Having computed $G^{M,x}$ and $G^{M,y}$, we recover the TE Green tensor from (9) and (10).

3 The computational methods

3.1 Boundary integrals and the boundary-integral-equation formulation

Since we have essentially the same types of equations for TM and TE polarizations, for clarity, we develop the computational method only for the TM case, although we present the computation results for both TM and TE polarizations. Our numerical method is based on the boundary-integral method, using potential theory and Green's theorem [5]. To obtain the desired integral equations, we look for solutions in the holes as layer potentials, apply Green's identity in the annulus regions, and write the solutions of the outer region as a sum of layer potentials.

Let us define the single- and double-layer potentials, for $l = 1, 2, \ldots, M$, and $j = 1, 2$, by

$$S_n^{l,j}\phi_l^j(\mathbf{x}) = 2\int_{\Gamma_l^j} \Phi_n^j(\mathbf{x},\mathbf{x}')\phi_l^j(\mathbf{x}')\,\mathrm{d}s(\mathbf{x}'), \quad \mathbf{x}\in\mathbf{R}^2\backslash\Gamma_l^j,$$

and

$$D_n^{l,j}\psi_l^j(\mathbf{x}) = 2\int_{\Gamma_l^j} \frac{\partial}{\partial\mathbf{N}(\mathbf{x}')}\Phi_n^j(\mathbf{x},\mathbf{x}')\psi_l^j(\mathbf{x}')\,\mathrm{d}s(\mathbf{x}'), \quad \mathbf{x}\in\mathbf{R}^2\backslash\Gamma_l^j,$$

respectively, for $n = 1, \ldots, M$. where the functions ϕ_l^j and ψ_l^j are the density functions. We also define $S_0^{l,j}$ and $D_0^{l,j}$ as above with Φ_n^j replaced by Φ_0. We denote by $P^{m,l,j}$ and $Q^{m,l,j}$ the normal derivatives of $S^{l,j}$ and $D^{l,j}$ at some point on a boundary Γ_m^j, $m \neq l$, respectively. Accordingly we denote by $S^{m,l,j}\phi(\mathbf{x})$ and $D^{m,l,j}\psi(\mathbf{x})$ the values of $S^{l,j}\phi(\mathbf{x})$ and $D^{l,j}\psi(\mathbf{x})$ when $\mathbf{x}$ belongs to Γ_m^j, $m \neq l$.

It is known (cf. [10] and [13, Sect. 2.7]) that the above-defined potentials are analytic in $\mathbf{R}^2\backslash\Gamma_l^j$ and, when $\mathbf{x}$ approaches Γ_l^j, $S^{l,j}$ and $Q^{l,j}$, are continuous whereas $D^{l,j}$ and $P^{l,j}$ exhibit jumps. In particular,we have on Γ_l^j,

$$S^{m,l,j} \to \hat{S}^{l,j}, \quad N^{m,l,j} \to \hat{N}^{l,j}, \tag{12}$$

$$D^{m,l,j} \to \mp I + \hat{D}^{l,j} \quad \text{and} \quad P^{m,l,j} \to \pm I + \hat{P}^{l,j}, \tag{13}$$

where the upper (lower) sign corresponds to the limit when $\mathbf{x}$ approaches Γ_l^j from outside (inside) and I is the identity operator. The compact operators $\hat{S}^{l,j}$, $\hat{P}^{l,j}$, $\hat{D}^{l,j} : C(\Gamma_l^j) \to C(\Gamma_l^j)$ are given, on Γ_l^j, by

$$\hat{S}_n^{l,j}\phi_l^j(\mathbf{x}) = \int_{\Gamma_l^j} \Phi_n(\mathbf{x},\mathbf{y})\phi_l^j(\mathbf{y})\,\mathrm{d}s(\mathbf{y}), \quad \mathbf{x}\in\Gamma_l^j, \tag{14}$$

$$\hat{P}_n^{l,j}\phi_l^j(\mathbf{x}) = \int_{\Gamma_l^j} \frac{\partial}{\partial\mathbf{N}(\mathbf{x})}\Phi_n(\mathbf{x},\mathbf{y})\phi_l^j(\mathbf{y})\,\mathrm{d}s(\mathbf{y}), \quad \mathbf{x}\in\Gamma_l^j, \tag{15}$$

$$\hat{D}_n^{l,j}\psi_l(\mathbf{x}) = \int_{\Gamma_l^j} \frac{\partial}{\partial\mathbf{N}(\mathbf{y})}\Phi_n(\mathbf{x},\mathbf{y})\psi_l^j(\mathbf{y})\,\mathrm{d}s(\mathbf{y}), \quad \mathbf{x}\in\Gamma_l^j \tag{16}$$

and the unbounded operator $\hat{N}_n^{l,j} : \Upsilon(\Gamma_l^j) \to C(\Gamma_l^j)$ is given, on Γ_l^j, by

$$\hat{N}_n^{l,j}\psi_l^j(\mathbf{x}) = \frac{\partial}{\partial \mathbf{N}(\mathbf{x})}\int_{\Gamma_l^j}\frac{\partial}{\partial \mathbf{N}(\mathbf{y})}\Phi_n(\mathbf{x},\mathbf{y})\psi_l(\mathbf{y})\,ds(\mathbf{y}), \quad \mathbf{x}\in\Gamma_l^j. \tag{17}$$

Here $C(\Gamma)$ is the linear space of all continuous functions on Γ, and $\Upsilon(\Gamma)$ is the linear space of all continuous functions ψ with the property that the double-layer potential with density ψ has continuous normal derivatives on both sides of Γ. It can be shown that $\hat{N}_m^{l,j} - \hat{N}_n^{l,j}$, $m \neq n$, is a compact operator in $C(\Gamma_l^j)$. We refer to [13, Sect. 2.7], for details and proof of compactness for the above operators.

Applying Green's theorem [14, Sect. 2.2], for $l = 1, \ldots, M$, we obtain

$$-2u_l^1(\mathbf{x}) = \sum_{j=1}^{2}\left(S_l^{l,j}\frac{\partial}{\partial \mathbf{N}}u_l^1(\mathbf{x}) - D_l^{l,j}u_l^1(\mathbf{x})\right), \quad \mathbf{x}\in\Omega_l^1 \tag{18}$$

and

$$0 = \sum_{j=1}^{2}\left(S_l^{l,j}\frac{\partial}{\partial \mathbf{N}}u_l^1(\mathbf{x}) - D_l^{l,j}u_l^1(\mathbf{x})\right), \quad \mathbf{x}\notin\Omega_l^1. \tag{19}$$

So, we obtain the field inside Ω_l^1 by (18) once we know it and its normal derivatives on the boundaries. For the holes Ω_l^2 and in the exterior domain Ω_0, we look for the fields as a combination of single- and double-layer potentials, i.e.,

$$u_l^2 = (S_l^{l,2} + \mathrm{i}\alpha D_l^{l,2})\phi_l^2, \quad \mathbf{x}\in\Omega_l^2, \quad l = 1, \ldots, M, \tag{20}$$

and

$$u_0 = \sum_{l=1}^{M}(S_0^{l,1} + \mathrm{i}\beta D_0^{l,1})\phi_l^1, \quad \mathbf{x}\in\Omega_0. \tag{21}$$

where α and β are positive real constants.

Using (12) and (13) we obtain on the boundaries, for $l = 1, \ldots, M$,

$$u_l^2 = \hat{Q}_l^{l,2}\phi_l^2, \quad \frac{\partial u_l^2}{\partial \mathbf{N}} = \hat{R}_l^{l,2}\phi_l^2 \quad \text{on } \Gamma_l^2, \tag{22}$$

and

$$u_0 = \hat{V}_0^{l,1}\phi_l^1 + \sum_{n\neq l}^{M}V_0^{l,n,1}\phi_n^1, \quad \frac{\partial u_0}{\partial \mathbf{N}} = \hat{W}_0^{l,1}\phi_l^1 + \sum_{n\neq l}^{M}W_0^{l,n,1}\phi_n^1 \quad \text{on } \Gamma_l^1. \tag{23}$$

where

$$\hat{Q}_l^{l,2} = \hat{S}_l^{l,2} + \mathrm{i}\alpha(\hat{D}_l^{l,2} + I), \quad \hat{R}_l^{l,2} = (\hat{P}_l^{l,2} - I) + \mathrm{i}\alpha\hat{N}_l^{l,2}$$
$$V_0^{l,n,1} = S_0^{l,n,1} + \mathrm{i}\beta D_0^{l,n,1}, \quad W_0^{l,n,1} = P_0^{l,n,1} + \mathrm{i}\beta N_0^{l,n,1},$$
$$\hat{V}_0^{l,1} = \hat{S}_0^{l,1} + \mathrm{i}\beta(\hat{D}_0^{l,1} - I) \quad \text{and} \quad \hat{W}_0^{l,1} = (\hat{P}_0^{l,1} + I) + \mathrm{i}\beta\hat{N}_0^{l,1}$$

By straightforward calculations we can see that u_0 given in (21) satisfies the Sommerfeld radiation condition.

Clearly, for $l = 1, \ldots, M$, and $j = 1, 2$, u_l^j and u_0 given in (18), (20) and (21) are solutions of (4) and (5), respectively.

Now, we obtain ϕ_l^j, for $l = 1, \ldots, M$, and $j = 1, 2$, from a system of boundary-integral equations, by using the boundary conditions (6) and (7) in (19).

In particular, to obtain the desired boundary-integral equations, we let $\mathbf{x}$ tend to the boundary in (19), using the boundary conditions (6) and (7), and jump properties of layer potentials (12) and (13). We then have

$$\hat{S}_l^{l,1}\frac{\partial u_0}{\partial \mathbf{N}} - (\hat{D}_l^{l,1} - I)u_0 + S_l^{1,l,2}\frac{\partial u_l^2}{\partial \mathbf{N}} - D_l^{1,l,2}u_l^2 = F_l \tag{24}$$

on Γ_l^1, where

$$F_l = \hat{S}_l^{l,1}\frac{\partial f_l^{1,0}}{\partial \mathbf{N}} - (\hat{D}_l^{l,1} - I)f_l^{1,0} + S_l^{1,l,2}\frac{\partial f_l^{1,2}}{\partial \mathbf{N}} - D_l^{1,l,2}f_l^{1,2},$$

and

$$S_l^{2,l,1}\frac{\partial u_0}{\partial \mathbf{N}} - D_l^{2,l,1}u_0 + \hat{S}_l^{l,2}\frac{\partial u_l^2}{\partial \mathbf{N}} - (I + \hat{D}_l^{l,2})u_l^2 = G_l \tag{25}$$

on Γ_l^2, where

$$G_l = S_l^{2,l,1}\frac{\partial f_l^{1,0}}{\partial \mathbf{N}} - D_l^{2,l,1}f_l^{1,0} + \hat{S}_l^{l,2}\frac{\partial f_l^{1,2}}{\partial \mathbf{N}} - (I + \hat{D}_l^{l,2})f_l^{1,2}.$$

Using (22) and (23) we can write (24) and (25) in a simplified form as

$$F_l = \hat{A}_0^{l,1}\phi_l^1 + \sum_{n=1,n\neq l}^{M} A_0^{l,n,1}\phi_n^1 + B_l^{1,l,2}\phi_l^2 \quad \text{on } \Gamma_l^1, \quad l = 1, 2, \ldots, M, \tag{26}$$

and

$$G_l = A_0^{2,l,1}\phi_l^1 + \sum_{n=1,n\neq l}^{M} A_0^{l,n,2}\phi_n^1 + \hat{B}_l^{l,2}\phi_l^2 \quad \text{on } \Gamma_l^2, \quad l = 1, 2, \ldots, M, \tag{27}$$

where

$$\hat{A}_0^{l,1} = \hat{S}_l^{l,1}\hat{W}_0^{l,1} - \left(\hat{D}_l^{l,1} - I\right)\hat{V}_0^{l,1},$$
$$A_0^{l,n,1} = \hat{S}_l^{l,1}\hat{W}_0^{l,n,1} - \left(\hat{D}_l^{l,1} - I\right)V_0^{l,n,1},$$
$$B_l^{1,l,2} = S_l^{1,l,2}\hat{R}_l^{l,2} - D_l^{1,l,2}\hat{Q}_l^{l,2},$$
$$A_0^{2,l,1} = S_l^{2,l,1}\hat{W}_0^{l,1} - D_l^{2,l,1}\hat{V}_0^{l,1},$$
$$A_0^{l,n,2} = S_l^{2,l,1}W_0^{l,n,1} - D_l^{2,l,1}V_0^{l,n,1},$$

and

$$\hat{B}_l^{l,2} = \hat{S}_l^{l,2}\hat{R}_l^{l,2} - (I + \hat{D}_l^{l,2})\hat{Q}_l^{l,2}.$$

Using the identity $\hat{S}_n^{l,j}\hat{N}_n^{l,j} = -I + \left(\hat{D}_n^{l,j}\right)^2$ [10] in $\hat{A}_0^{l,1}$ and $\hat{B}_l^{l,2}$ we observe that the system (26), (27) is of Fredholm type. It is straightforward to see that the boundary conditions (6) and (7) are satisfied if $\phi_l^j, l = 1, 2, \ldots, M$ and $j = 1, 2$ are solutions of (26) and (27). The unique solvability follows from Riesz–Fredholm theory [10].

3.2 Parametrization and discretization

The boundaries Γ_l^j, $l = 1, 2, \ldots, M$, and $j = 1, 2$ are assumed to possess regular analytic and 2π-periodic representation of the form

$$\mathbf{x}_l^j(t) = \left(\mathbf{x}_{l,1}^j(t), \mathbf{x}_{l,2}^j(t)\right), \quad 0 \le t \le 2\pi, \tag{28}$$

in counterclockwise orientation, such that, the unit outward normal $\mathbf{N}\left(\mathbf{x}_l^j\right) := \mathbf{N}_l(\mathbf{x})$ is written as

$$\mathbf{N}\left(\mathbf{x}_l^j(t)\right) = \frac{1}{\left|\mathbf{x}_l^{j\,\prime}(t)\right|}\mu_l(t), \tag{29}$$

where,

$$\mu_l(t) := \begin{pmatrix} \mathbf{x}_{l,2}^{j\,\prime}(t) \\ -\mathbf{x}_{l,1}^{j\,\prime}(t) \end{pmatrix}.$$

Then, we write $S^{m,l,j}$, $D^{m,l,j}$, $P^{m,l,j}$ and $N^{m,l,j}$ in the form

$$\mathbf{U}_n^{m,l,j}\left(\phi\mathbf{x}_m(t)\right) = -\frac{\mathrm{i}}{2}\int_0^{2\pi} U_n\left(\mathbf{x}_m(t), \mathbf{x}_l^j(\tau)\right)\phi(\mathbf{x}_l^j(\tau))|\mathbf{x}_l^{j\,\prime}(\tau)|\,\mathrm{d}\tau, \tag{30}$$

where the kernel $U_n(\mathbf{x}, \mathbf{y})$ is given by

$$U_n(\mathbf{x},\mathbf{y}) = \begin{cases} H_0^{(1)}(\kappa_n|\mathbf{x}-\mathbf{y}|) & \text{when } \mathbf{U}_n^{m,l,j} = S_n^{m,l,j} \\ \frac{\partial}{\partial\mathbf{N}(\mathbf{y})}H_0^{(1)}(\kappa_n|\mathbf{x}-\mathbf{y}|) & \text{when } \mathbf{U}_n^{m,l,j} = D_k^{m,l,j} \\ \frac{\partial}{\partial\mathbf{N}(\mathbf{x})}H_0^{(1)}(\kappa_n|\mathbf{x}-\mathbf{y}|) & \text{when } \mathbf{U}_n^{m,l,j} = P_n^{m,l,j} \\ \frac{\partial}{\partial\mathbf{N}(\mathbf{x})}\left(\frac{\partial}{\partial\mathbf{N}(\mathbf{y})}H_0^{(1)}(\kappa_n|\mathbf{x}-\mathbf{y}|)\right) & \text{when } \mathbf{U}_n^{m,l,j} = N_n^{m,l,j} \end{cases} \tag{31}$$

The Nyström's method replaces the integrals in (30) by integrals of the trigonometric interpolation polynomials with respect to τ of the integrands. In particular, for $M \in \mathbf{N}$ and $t_n = \pi n/M$, $n = 0, \ldots, 2M-1$, the integrals of the form $\int_0^{2\pi} f(\tau)\,\mathrm{d}\tau$ are approximated such that

$$\int_0^{2\pi} f(\tau)\,\mathrm{d}\tau \approx \frac{\pi}{M}\sum_{n=0}^{2M-1} f(t_n). \tag{32}$$

For $m \neq l$ we can use (32) to derive a discretized form of $\mathbf{U}_n^{m,l,j}$.

We discretize the boundary integrals (14)–(17) by the exponentially converging Nyström method (Cf. [14, Sect. 3.5] and [15].

3.3 The numerical and semi-analytical algorithms

The problem (26), (27) will then have a discrtized form. The resulting matrix equation is solved by a multigrid method [16, Chap. 14]. The numerous matrix–vector multiplication can be done efficiently by a fast multipole method [17].

Finally, we describe briefly the semi-analytical method used for validation. For more details, we refer to [1]. If the finite-size PC is composed of circular rods and circular holes, a closed-form solution can be derived. We take the solution of the hole domains as an infinite expansion of Bessel functions of the first kind, the solutions in the annular regions as an expansion of Bessel functions of the first kind and Hankel functions of the first kind, and the solution of the outer region as an expansion of Hankel functions of the first kind. Then, using the boundary conditions and the Graf formula, we obtain an infinite system. This system is truncated and a multigrid method is used for approximating the solution.

4 Computational results

We assume a crystal with a hexagonal symmetry (Fig. 1), composed of a set of dielectric cylinders which are either circular with radius $r = 0.6$ or square of the same size (the side is equal to the diameter of the circular geometry), spacing constant (distance between the centers of the closest cylinders) $d = 4$ (see Fig. 2), wavelength λ, $\nu_0 = 1$,

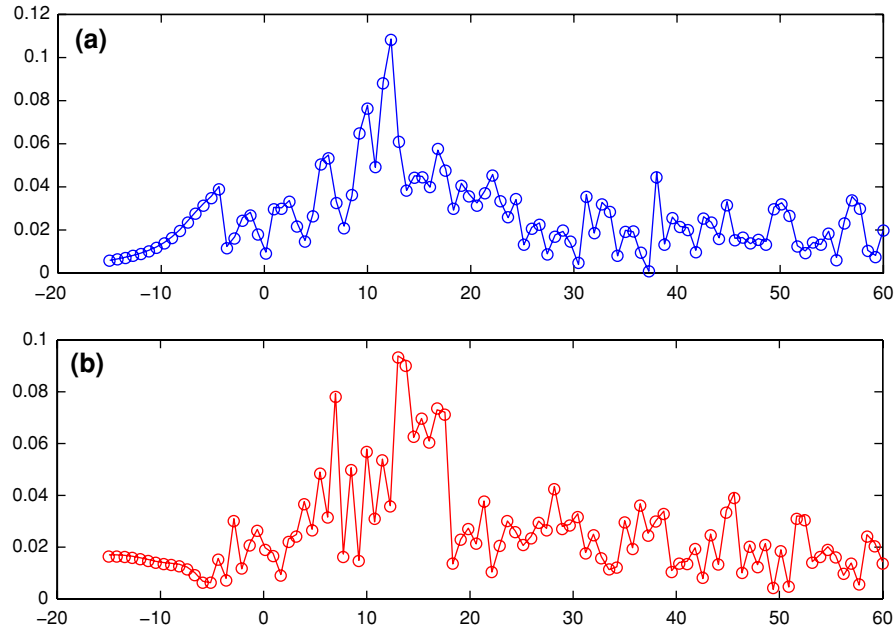

Fig. 3 The absolute value of the Green tensor components G_{xx} (**a**) and G_{yx} (**b**) against the x-coordinate for a wave length $\lambda = 3.05$ by the numerical method (*solid line*) and semi-analytical result (o) for an annular crystal case CC composed of 85 rods, using holes with radius $r_0 = 0.2$

$\nu_l^2 = 1$, and $\nu_l^1 = 2.9$, $l = 1, \ldots, M$. The holes are either circular with radius r_0 or deformed circles of the same size.

The first numerical result we want to present is the computation of the Green tensor components for a CC case annular PC composed of 85 dielectrics. In Figs. 3 and 4 we plot G_{xx}, G_{yx}, and G_{yy}, G_{zz}, respectively, for $\lambda = 3.05$, using the semi-analytical and the boundary-integral methods. We observe a very a good match of the two methods for all the components.

Having validated all the Green-tensor components for TE and TM cases, in the sequel we only consider the latter. In particular, we will compute and analyze G^{TM} for various configurations.

For the above-mentioned parameter values, when we vary the radius of the hole from $r_0^1 = 0.1$ to $r_0^2 = 0.3$, it is known [8] that the gap interval shrinks for wavelengths from approximately [7.3, 10.6] to approximately [7.3, 9.5]. In Fig. 5, when we compute the Green tensor for a point source placed in the crystal using $\lambda = 10.4$ for r_0^1 and r_0^2, we see, first of all, a very good match between the numerical and the semi-analytical results. Secondly, we observe that the Green tensor decays much faster outside the crystal for r_0^1 in contrast to r_0^2. This is expected since it means (cf. [18]) that for the hole radius r_0^1, $\lambda = 10.45$ lies within the gap, whereas for r_0^2 it does no longer belong to the bandgap. Note that there is no symmetry in the figures since the source is placed randomly in the crystal.

Now, for a fixed wavelength $\lambda = 8.05$, two different values of r_0 ($r_0 = 0.2$ and $r_0 = 0.5$), and a source located in the PC we plot the absolute value of the Green tensor on the x-coordinate using the semi-analytical and the numerical methods in the CC case of crystal containing 17 and 49 rods. The result is reported in Fig. 6.

We see, in all the cases, a very good match between the numerical and the semi-analytical results. We also see that the Green tensor decays much faster outside the crystal for $r_0 = 0.2$ than for $r_0 = 0.5$. This means that, for the radius $r_0 = 0.5$, $\lambda = 8.05$ does no longer belong to the bandgap. Moreover he result converges when the number of rods is increased.

In Fig. 7 we do the same numerical computations as in Fig. 6 for the cases CD, SC, and SD where the semi-analytical computation cannot be applied.

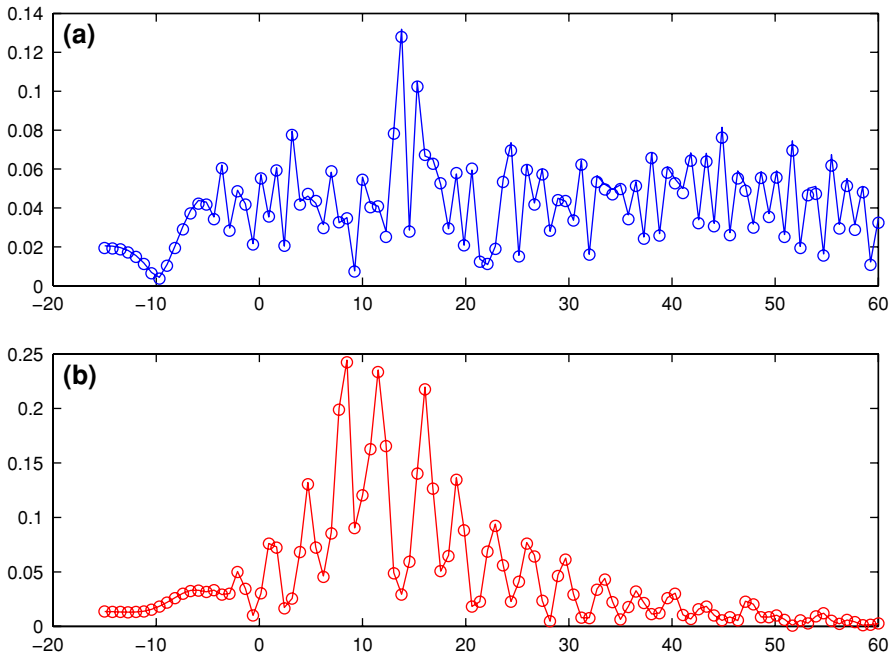

Fig. 4 The absolute value of the Green tensor components G_{yy} (**a**) and G_{zz} (**b**) against the x-coordinate for a wave length $\lambda = 3.05$ by the numerical method (*solid line*) and semi-analytical result (o) for an annular crystal case CC composed of 85 rods, using holes with radius $r_0 = 0.2$

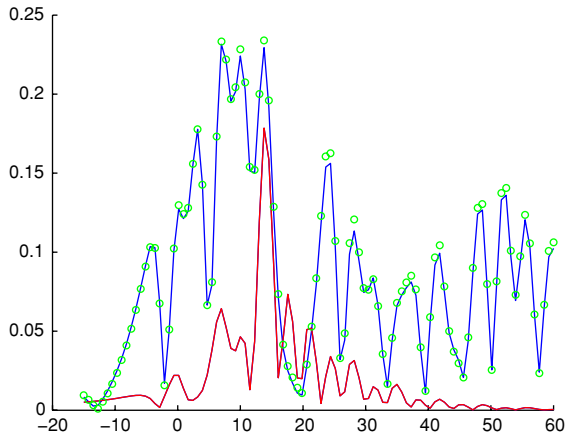

Fig. 5 The absolute value of the TM Green tensor against the x-coordinate for a wave length $\lambda = 10.4$ by the numerical method (*solid line*), in an annular crystal case CC for 85 rods, using a hole with radius 0.1 (*red*) and 0.3 (*blue*). The semi-analytical result is shown for the latter case (o), where we see a good match with the numerical solution

We see that the results are very similar in the four cases for $r_0 = 0.2$, whereas they are different in all cases for $r_0 = 0.5$. This suggests that a small deformation in the geometry (rods and/or holes) should not have serious impact on the bandgap.

Finally, for a source point placed in the crystal, we consider the behavior of the Green tensor when the hole radius varies. We study two cases: when the evaluation of the Green tensor is at a point within the crystal (Fig. 8) and when it is at a point far away from the crystal (Fig. 9). We know, from our analysis above, that in the latter case the absolute value of the Green tensor must be very small for a wavelength within the bandgap.

Let us consider two configurations of the geometry: the cases CC and SD. We see in Fig. 8 that, in both CC and SD cases, for a wavelength out of the bandgap for $r_0 = 0$ ($\lambda = 3.05$) the absolute value of the Green tensor oscillates, whereas for a wavelength within the bandgap for $r_0 = 0$ ($\lambda = 8.05$) the absolute value of the Green

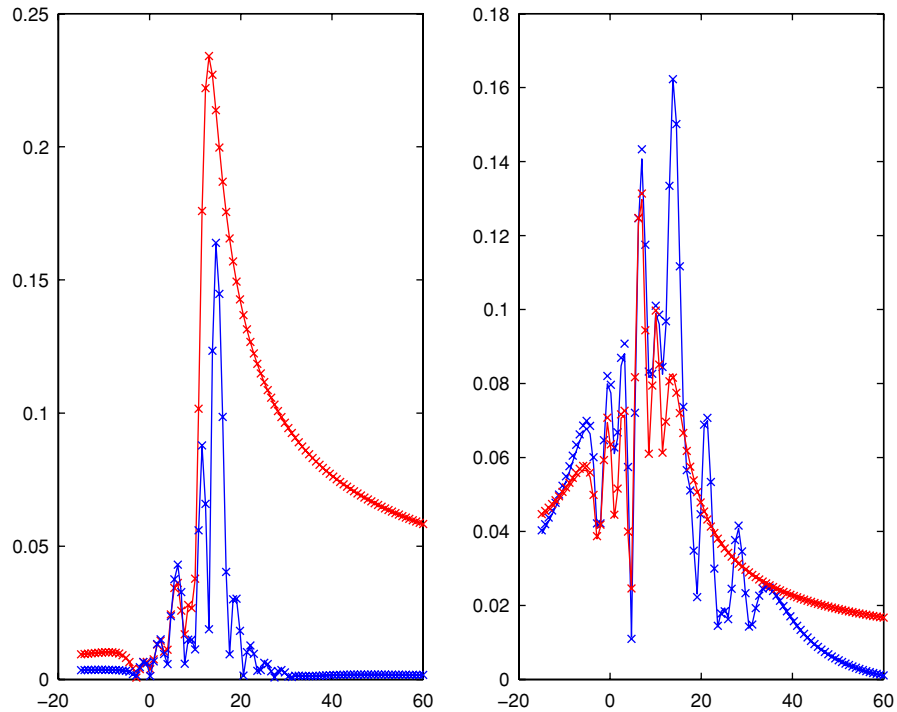

Fig. 6 In the two figures we plot the absolute value of the TM Green tensor against the x-coordinate for a wave length $\lambda = 8.05$ using the semi-analytical (–) and the numerical methods (x), in an annular crystal case CC for 17 rods (*red*) and 49 rods (*blue*). The figure on the left is the case when the hole has radius 0.2, and the figure on the right consists of the case when the hole has radius 0.5

tensor is smooth with only one minimum. However, the location of the minimum is different for the CC and SD cases.

In Fig. 9 where the Green tensor is evaluated far away from the crystal the observation is different than the previous case only for $\lambda = 8.05$. Indeed, in the CC configuration, we see that the absolute value of the Green tensor grows slowly until it reaches values comparable to its evaluation at points inside the crystal, then decays very fast and grows back. This suggests, as mentioned in [2], that by increasing r_0 the gap closes and after a threshold of r_0 it reopens. This observation does not occur for the SD case. Hence the bandgap formed after a threshold radius may be sensitive to small deformation in the geometry.

5 Conclusions

We have considered a two-dimensional annular photonic crystal of different geometrical configurations, which has a structure sketched in Figs. 1 and 2. The vector character of the fields in the Maxwell's equations implies that one has to distinguish two possible polarization directions with differing boundary conditions. The situation where the electric (resp. magnetic) field is parallel to the cylinders (z)-axis is called TM (resp. TE) polarization, with the magnetic (resp. electric) field thus being transverse.

We computed and analyzed the Green tensor for given source placed within the structure and an observation point. The TM and TE cases were both considered. For TM polarization the Green tensor reduces to a form involving only a single non-trivial scalar, while for TE polarization it reduces to a 2×2 tensor.

The numerical method used is the boundary-element technique based on potential theory and Green identities. We derived the boundary-integral equations that could be uniquely solvable using Riesz–Fredholm theory.

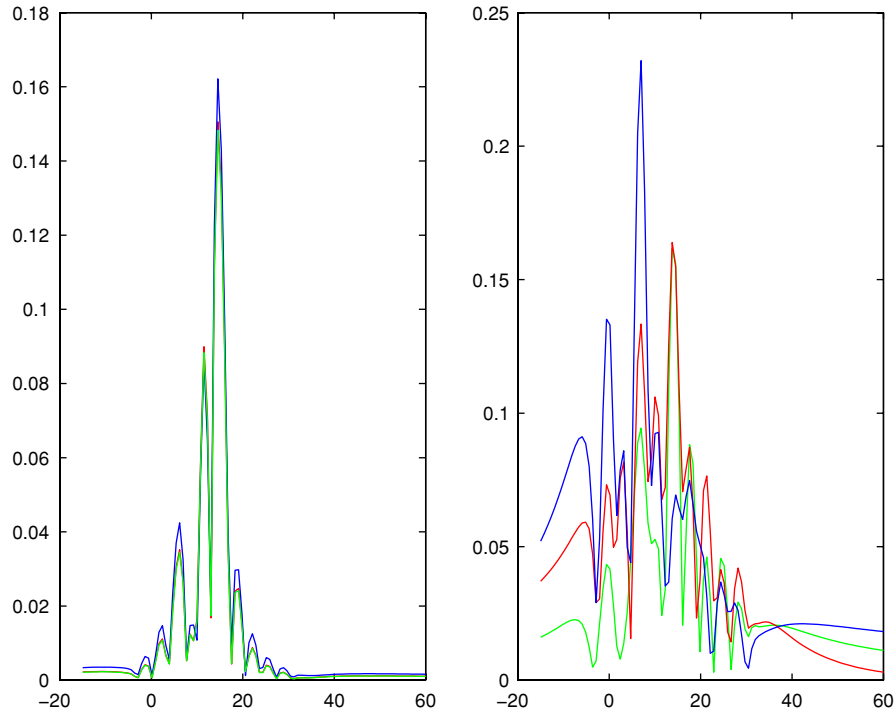

Fig. 7 In the two figures we plot the absolute value of the TM Green tensor against the x-coordinate for a wave length $\lambda = 8.05$. In both figures the numerical solution is computed for the cases of 'SC' (*red*), 'CD' (*blue*) and 'SD' (*green*). The figure on the left is the case when the hole is either circular with radius $r_0 = 0.2$ or a deformed circle of the same size, and the figure on the right consists of the case when the hole is either circular with radius $r_0 = 0.5$ or a deformed circle of the same size

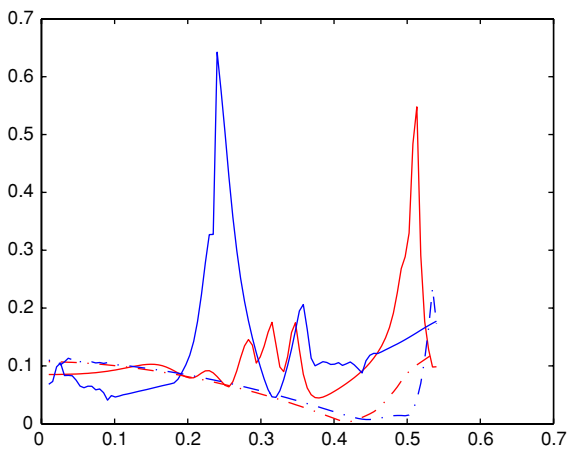

Fig. 8 The absolute value of the TM Green tensor evaluated at a point in the crystal against the radius of the hole r_0 for a source placed in the crystal. The solid red (resp. *blue*) is the case of CC (resp. SD) for $\lambda = 3.05$. The dashed red (resp. *blue*) is the case of CC (resp. SD) for $\lambda = 8.05$

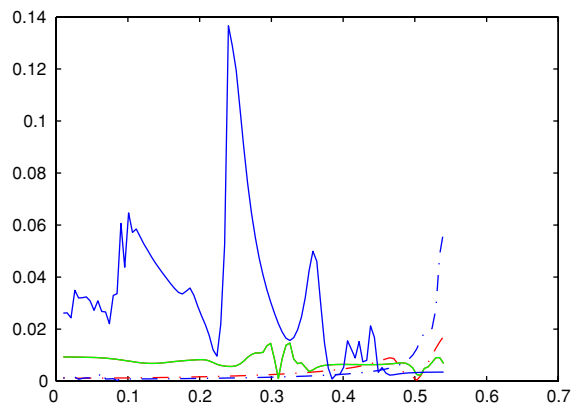

Fig. 9 The absolute value of the TM Green tensor evaluated at a point far from the crystal against the radius of the hole r_0 for a source placed in the crystal. The solid green (resp. *blue*) is the case of CC (resp. SD) for $\lambda = 3.05$. The dashed red (resp. *blue*) is the case of CC (resp. SD) for $\lambda = 8.05$

The boundary integrals use the free-source Green's function and inherit from its properties. The method requires matrix–vector multiplications, which can be efficiently done by available fast multipole methods.

Our numerical results show an excellent match between the semi-analytical calculations and the numerical method developed here.

For all the different geometrical configurations used, if we use two different values r_0^1 and r_0^2, with $r_0^1 < r_0^2$, for the radius of the hole, the gap interval shrinks. When we compute the Green tensor for a point source placed in the crystal using a wavelength within the bandgap, we observe that the Green tensor decays much faster outside the crystal in contrast to the case when the wavelength does no longer belong to the bandgap. This suggests that for certain values of the hole radius the Green tensor is not sensitive to the geometry.

Our results also suggest that, when increasing the radius of the hole, the gap closes and after a certain threshold it reopens. But the value of this threshold radius is sensitive to the geometry. Further studies will be necessary to establish the safety of this effect.

An experimental verification of some results obtained in this paper and the analysis in the three-dimensional case for non-spherical shapes are considered in our future work.

References

1. Kuhlmey BT, Pathmanandavel K, McPhedran RC (2006) Multipole analysis of photonic crystal fibers with coated inclusions. Opt Express 14:10851–10864
2. Kurt H, Citrin DS (2005) Annular photonic crystals. Opt Express 13:10316–10326
3. Wang SW, Lu W, Chen XS, Li ZF, Shen XC, Wen XC (2003) Two-dimensional photonic crystal at THz frequencies constructed by metal-coated cylinders. J Appl Phys 93:9401–9403
4. Stone JM, Pearce GJ, Luan F, Birks TA, Knight JC, George AK, Bird DM (2006) An improved photonic bandgap fiber based on an array of rings. Opt Express 14:6291–6296
5. Seydou F, Ramahi OM, Duraiswami R, Seppänen T (2006) Numerical computation of the Greenć6s function for two dimensional finite size photonic crystals of infinite length. Opt Express 14:11362–11371
6. van de Water AM, de Hon BP, van Beurden MC, Tijhuis AG, de Maagt P (2005) Linear embedding via Green's operators: a modeling technique for finite electromagnetic band-gap structures. Phys Rev E 72:056704
7. Dobson DC (1999) An efficient method for band structure calculations in 2D photonic crystals. J Comput Phys 149:363–376
8. Li EP, Wang QX, Zhang YJ, Ooi BL (2005) Analysis of finite-size coated electromagnetic bandgap structure by an efficient scattering matrix method. IEEE J Sel Top Qunantum Electron 11:485–492
9. Kress R, Roach G (1978) Transmission problems for the Helmholtz equation. J Math Phys 19:1433–1437
10. Kleinman R, Martin P (1988) On single integral equations for the transmission problem of acoustics. SIAM J Appl Math 48:307–325
11. Martin OJF, Piller NB (1998) Electromagnetic scattering in polarizable backgrounds. Phys Rev E 58:3909
12. Asatryan AA, Busch K, McPhedran RC, Botten LC, de Sterke CM, Nicorovici NA (2003) Two-dimensional Green tensor and local density of states in finite-sized two-dimensional photonic crystals. Wave Random Media 13:9–25
13. Colton D, Kress R (1983) Integral equation methods in scattering theory. John Wiley, New York
14. Colton D, Kress R (1998) Inverse acoustic and electromagnetic scattering theory. Springer-Verlag, Berlin
15. Kress R (1995) On the numerical solution of a hypersingular integral equation in scattering theory. J Comp Appl Math 61:345–360
16. Kress R (1999) Linear integral equations. Springer, New York
17. Song JM, Chew WC (2001) FMM and MLFMA in 3D and fast Illinois solver code. In: Chew WC, Jin J-M, Michielssen E, Song JM (eds) Fast and efficient algorithms in computational electromagnetics. Artech House, Norwood
18. Asatryan AA, Busch K, McPhedran RC, Botten LC, Martijn de Sterke C, Nicorovici NA (2001) Two-dimensional Green function and local density of states in photonic crystals consisting of a fnite number of cylinders of infnite length. Phys Rev E 63:046612